A&A 534, A126 (2011)
DOI: 10.1051/0004-6361/201117462

Astronomy & Astrophysics

X-ray spectroscopy of the Compton-thick Seyfert 2 ESO 138−G1

E. Piconcelli[1], S. Bianchi[2], C. Vignali[3], E. Jiménez-Bailón[4], and and F. Fiore[1]

[1] Osservatorio Astronomico di Roma (INAF), via Frascati 33, 00040 Monteporzio Catone (Roma), Italy
e-mail: piconcelli@mporzio.astro.it
[2] Dipartimento di Fisica, Università degli Studi Roma 3, via della Vasca Navale 84, 00146 Roma, Italy
[3] Dipartimento di Astronomia, Università di Bologna, via Ranzani 1, 40127 Bologna, Italy
[4] Instituto de Astronomia, Universidad Nacional Autónoma de México, Apartado Postal 70-264, 04510 Mexico DF, Mexico

Received 10 June 2011 / Accepted 1 August 2011

ABSTRACT

We report on our analysis of *XMM-Newton* observations of the Seyfert 2 galaxy ESO 138−G1(z = 0.0091). These data reveal a complex spectrum in both its soft and hard portions. The 0.5−2 keV band is characterized by a strong "soft-excess" component with several emission lines, as commonly observed in other narrow-line AGN. Above 3 keV, a power-law fit yields a very flat slope ($\Gamma \sim 0.35$), along with the presence of a prominent line-like emission feature around ∼6.4 keV. This indicates heavy obscuration along the line of sight to the nucleus. We find an excellent fit to the 3−10 keV continuum with a pure reflection model, which provides strong evidence of a Compton-thick screen, preventing direct detection of the intrinsic nuclear X-ray emission. Although a model consisting of a power law transmitted through an absorber with $N_{\rm H} \sim 2.5 \times 10^{23}$ cm^{-2} also provides a reasonable fit to the hard X-ray data, the equivalent width (EW) value of ∼800 eV measured for the Fe Kα emission line is inconsistent with a primary continuum obscured by a Compton-thin column density. Furthermore, the ratio of 2−10 keV to de-reddened [OIII] fluxes for ESO 138−G1 agrees with the typical values reported for well-studied Compton-thick Seyfert galaxies. Finally, we also note that the upper limits to the 15−150 keV flux provided by Swift/BAT and INTEGRAL/IBIS seem to rule out the presence of a transmitted component of the nuclear continuum even in this very hard X-ray band, hence imply that the column density of the absorber could be as high as 10^{25} cm^{-2}. This makes ESO 138−G1 a very interesting, heavy Compton-thick AGN candidate for the next X-ray missions with spectroscopic and imaging capabilities above 10 keV.

Key words. galaxies: active – galaxies: nuclei – X-ray: galaxies – galaxies: individual: ESO 138−G1

1. Introduction

Since X-ray radiation is emitted from within a few gravitational radii of the SMBH, it can provide insights into AGN activity with unrivalled detail. Furthermore, typical X-ray observations in the 2−10 keV range easily penetrate regions (i.e. dust lanes, the torus, star-forming knots) with high extinction in optical ($A_{\rm V} > 50$ mag) located along our line-of-sight to the nucleus. The census of AGN in the Universe is, however, still incomplete as illustrated by the mismatch between the total mass function of local SMBHs and the SMBH mass function inferred from the X-ray-selected AGN luminosity functions (Marconi et al. 2004), and because only ∼60% of the cosmic X-ray background in the 5−10 keV band has been so far resolved into point sources (Worsley et al. 2005).

It is well-known that one of the major difficulties to overcome is the detection of the most elusive AGN, i.e. those suffering heavy obscuration (i.e. with column density of $N_{\rm H} \gtrsim \sigma_t^{-1} \approx 1.6 \times 10^{24}$ cm^{-2}), the so-called Compton-thick (CT) AGN. As the primary continuum is blocked, their X-ray emission below 10 keV is mainly due to the Compton reflection and fluorescence from optically-thick circumnuclear material (Matt 1997). Accordingly, the observed 2−10 keV fluxes for CT AGN therefore represent only 1–10% of their intrinsic fluxes. The typical 2−10 keV reflection-dominated spectrum is flat and characterized by a prominent ($EW \gtrsim 0.6$−1 keV) Fe Kα emission line at 6.4 keV.

According to the X-ray background synthesis models (e.g., Gilli et al. 2007) and direct estimates from local samples of galaxies (Risaliti et al. 1999; Cappi et al. 2006; Malizia et al. 2009; Burlon et al. 2011), CT AGNs should account for ∼20−30% of the entire AGN population. Nonetheless, only a few dozen of them (mostly local, low-luminosity Seyfert galaxies) have been unambiguously discovered and studied so far (Comastri 2004; Fukazawa et al. 2011; Della Ceca et al. 2008, and references therein). Furthermore, ultra-deep X-ray exposures have provided clear evidence of powerful CT quasars at high redshifts (e.g., Feruglio et al. 2011; Comastri et al. 2011; Gilli et al. 2011; Fiore et al. 2011), whose existence has been debated for many years (e.g., Halpern et al. 1999). Enlarging the sample of well-studied CT AGNs in the X-ray regime is therefore useful to characterize their properties more accurately, confirm distinctive spectral features, and strengthen the relations between optical/IR and X-ray observable quantities of this elusive class of X-ray sources.

In this paper, we study the X-ray spectral properties of ESO 138−G1, a Seyfert 2 galaxy at z = 0.0091. This AGN is hosted in an E/S0 galaxy that has a peculiar morphology of a bulge surrounded by a ring, within which there is a hint of a bar (Alloin et al. 1992; Ferruit et al. 2000). Furthermore, ESO 138−G1 exhibits a compact nucleus and a bright asymmetric, wedge-shaped circumnuclear zone of diffuse light resembling an ionization cone from the AGN (Munoz-Marin et al. 2007). All these features make ESO 138−G1 a unusual

and particularly interesting object. On the basis of *ASCA* data, Collinge & Brandt (2000) found a hard spectrum ($\Gamma \approx 0.5$) and a strong Fe Kα emission line, implying that this Seyfert 2 galaxy is Compton-thick/reflection-dominated. However, statistically acceptable fits can also be achieved using a partial-covering absorption column of $N_{\rm H} = 2 \times 10^{23}$ cm^{-2}. Here, we present and discuss the results of our analysis of two archival *XMM-Newton* spectroscopic observations of ESO 138−G1.

2. *XMM-Newton* observations and data reduction

ESO 138−G1 was observed by *XMM-Newton* (Jansen et al. 2001) on 2007 February 16 (Obs. ID: 0405380201) and 2007 March 25 (Obs. ID: 0405380901). Both observations were performed with the *EPIC* cameras operating in full-frame mode.

Data were reduced with SAS 11.0 (Gabriel et al. 2004) using standard procedures. We selected X-ray events corresponding to patterns 0–4(0–12) for the PN(MOS) camera. The event lists were filtered to ignore periods of high background flaring according to the method presented in Piconcelli et al. (2004) based on the cumulative distribution function of background light-curve count-rates. For the PN detector, source counts were extracted from a circular region with a radius of 30 arcsec (14 arcsec for the 901 observation since it was affected by a higher background level). Background counts were estimated from a 50 arcsec-radius region on the same chip for both datasets. After screening the final net exposure times are 15.5 and 11.4 ks for the 201 and 901 observation, respectively. The redistribution matrix files and ancillary response files were created using the SAS task RMFGEN and ARFGEN, respectively. During the *XMM-Newton* observations, ESO 138−G1 did not display any variation in either X-ray flux and the spectral shape, thus we coadded the PN spectra to increase the signal-to-noise ratio and created a combined response matrix. Source and background spectra were summed using the FTOOL task *mathpha*[1].

The combined PN spectrum was rebinned so that each energy bin contained at least 25 counts to allow us to use the χ^2 minimization technique in spectral fitting.

The reduction of MOS spectra was carried out following the same procedure applied to the PN datasets. We adopted an extraction radius of 31 arcsec for the source spectra, while the background counts were extracted from neighbouring source-free circular regions with a radius of 50 arcsec.

In this paper, we focus on the analysis of PN spectroscopic data only because of the higher sensitivity of this detector over the broad 0.5−10 keV range than both MOS cameras (even when they are combined), and above 5 keV in particular. Nevertheless, we checked that consistent results were obtained including the MOS data in our analysis. Finally, no useful high resolution RGS data (den Herder et al. 2001) were obtained from the present *XMM-Newton* observations of ESO 138−G1 because of their short exposure times.

3. X-ray spectral analysis

We analyzed the spectra with the XSPEC v12.5 package (Arnaud 1996). We limited our analysis to the 0.5−10 keV energy range, where the accuracy of the *EPIC* calibrations is maximal. All models presented in this paper include absorption caused by the line-of-sight Galactic column density of $N_{\rm H} = 1.3 \times 10^{21}$ cm^{-2} (Kalberla et al. 2005).

We provide best-fit parameter values in the source frame, unless otherwise specified. The quoted errors in the model parameters correspond to a 90% confidence level for one interesting parameter ($\Delta\chi^2 = 2.71$; Avni 1976). In this work, we assume a ΛCDM cosmology with $H_0 = 70$ km s^{-1} Mpc^{-1} and $\Omega_\Lambda = 0.73$ (e.g., Larson et al. 2011).

3.1. Hard X-ray band and Fe Kα lines

The 0.5–10 keV *EPIC* PN spectrum of ESO 138−G1 is shown in Fig. 1a. Owing to its complexity, we first studied the X-ray spectrum in the 3.5−10 keV band to gain insight into the origin of the X-ray emission in this energy range. This emission should be relatively unaffected by the extended photoionized/scattered "soft excess" component frequently observed in obscured AGNs (Turner et al. 1997; Sambruna et al. 2001; Bianchi et al. 2007), which we consider in Sect. 3.2. As expected for a highly absorbed Seyfert 2 galaxy, a fit to the PN spectrum with a simple power-law in the 3.5−10 keV band (excluding the 6−7.5 keV Fe K energy range) reveals a very flat spectral shape with a photon index $\Gamma \sim 0.35$. We tested two alternative scenarios for the hard X-ray spectrum of ESO 138−G1: (i) a reflection-dominated (RD) one, where the X-ray primary continuum from the AGN is totally depressed in the *EPIC* band, as expected in case of a CT absorber; and (ii) a transmission-dominated (TD) scenario, where the AGN emission is absorbed by a Compton-thin (i.e., $N_{\rm H} < 10^{24}$ cm^{-2}) obscuring screen that only moderately suppresses the X-ray continuum in the 3.5−10 keV range. Moreover, we explore a scenario wherein both reflection and transmission components are present.

In Fig. 1b, we show the hard X-ray PN spectrum fitted by the best-fit RD model, which consists of a cold reflection component, modeled by `PEXRAV` in XSPEC. In this modelling, we assumed that $\Gamma = 1.8$, that the reflection scaling factor $R = -1$ (defined as $R = \Omega/2\pi$, where Ω is the solid angle subtended by the reflector for isotropic incident emission; Magdziarz & Zdziarski 1995), that the metal abundances of the reflector were fixed to their solar values and that the inclination angle was fixed to 65 deg. The RD model also included a strong fluorescent Fe Kα emission line close to 6.4 keV, plus three narrow Gaussian lines at 6.63, 7.058, and 7.54 keV associated with He-like Fe Kα, Fe Kβ, and Ni Kα emission, respectively. The addition of each Fe and Ni Kα line produces an improvement in the resulting fit statistic significant at ≥99% confidence level (94% in the Fe Kβ line case) according to an $F-$test. We fitted the Compton shoulder (CS) to the Fe Kα line by adding a Gaussian emission line at 6.3 keV with $\sigma \equiv 40$ eV and a normalization fixed to 20% of the neutral Fe Kα line as expected for CT material (e.g., Matt et al. 2002; Yaqoob & Murphy 2011). The CS redwards of 6.4 keV is emitted from neutral material as a result of Compton downscattering of the Fe line photons in the same medium. The addition of the CS component reduces the χ^2 fit statistic of $\Delta\chi^2 = 6$. The RD model gives a very good fit to the data with a $\chi^2(\nu) = 78(75)$ (see Table 1).

The TD model yields a reasonable fit to the *XMM-Newton* data with a final $\chi^2(\nu) = 83(73)$. The spectrum is described by an absorbed continuum power-law with $\Gamma = 1.9 \pm 0.4$ and $N_{\rm H} = 2.4^{+0.3}_{-0.4} \times 10^{23}$ cm^{-2} (see Table 1). As for the model RD, four narrow Gaussian lines (i.e., neutral Fe Kα, He-like Fe Kα, Fe Kβ, and Ni Kα) are included in the fit. When we add a CS component to the fit that a normalization equal to 10% of the Fe Kα line core (as expected for a column density

[1] Spectral files were combined following the method outlined in http://heasarc.gsfc.nasa.gov/docs/asca/bgd_scale/bg_scale.html.

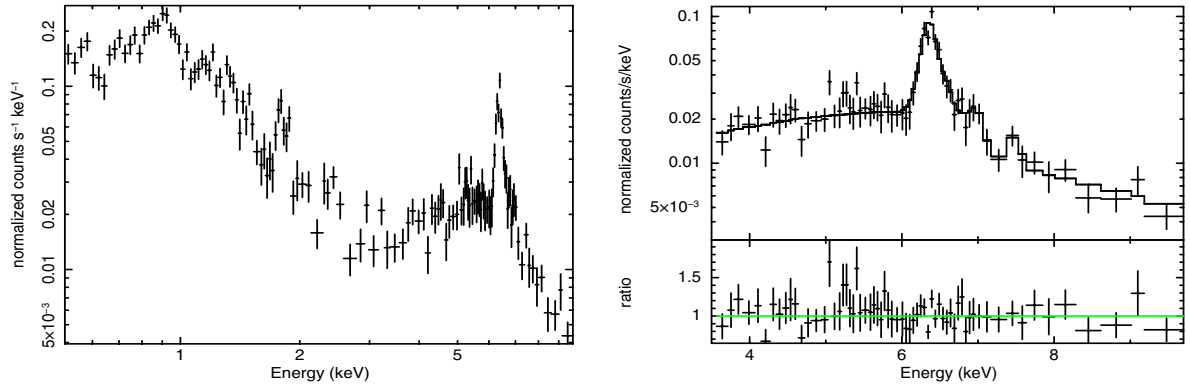

Fig. 1. (a) *Left*: *XMM-Newton* PN spectrum resulting from the merging of the 2007 February and March observations of ESO 138−G1. (b) *Right*: the RD model fitted to the 3.5−10 keV spectrum of ESO 138−G1. This model consists of a Compton reflection continuum component and five Gaussian lines accounting for the neutral Fe Kα line, its Compton shoulder, and the He-like Fe Kα, Fe Kβ, and Ni Kα emission lines, respectively. The bottom panel shows the data-to-model ratios.

Table 1. Best-fit spectral parameters for the hard X-ray (3.5−10 keV) continuum of ESO 138−G1.

Parameter	Model RD†	Model TD†
Γ^{a}	$1.8^{\ddagger}$	$1.9^{+0.4}_{-0.4}$
Norm^{b}	$8.2^{+0.4}_{-0.4}$	$1.6^{+1.3}_{-0.8}$
$N^{c}_{\rm H}$	–	$2.4^{+0.3}_{-0.4}$
F^{d}_{2-10}	2.3	2.1
L^{e}_{2-10}	4.3	9.6
χ^2_ν(d.o.f.)^{f}	1.04(75)	1.14(73)

Notes. See Sect. 3.1 for details. $^{(\dagger)}$ Spectral model: RD (*reflection*-dominated), TD (*transmission*-dominated); $^{(a)}$ photon index of primary continuum; $^{(b)}$ normalization of the reflection (RD) or absorbed power-law component (TD) (10^{-3} photons keV^{-1} cm^{-2} s^{-1} at 1 keV); $^{(c)}$ column density of the absorber (10^{23} cm^{-2}); $^{(d)}$ 2–10 keV flux (10^{-12} erg cm^{-2} s^{-1}); $^{(e)}$ 2–10 keV luminosity (10^{41} erg s^{-1}); $^{(f)}$ reduced χ^2 and number of degrees of freedom. $^{(\ddagger)}$ Fixed value (see text for details).

of $\sim$2.5 × 10^{23} cm^{-2}; Yaqoob & Murphy 2011), we achieve a $\Delta\chi^2 = 4$.

We investigated whether a clumpy absorber might be present along our line of sight by adding an absorbed power-law component to the TD model. The two power laws had the same photon index, thus mimicking a scenario wherein the obscuring screen along our line of sight is not uniform (e.g., Elitzur 2008; Ramos-Almeida et al. 2009). The fit resulted in $\chi^2(\nu)$ = 75(71), with an unusual steep continuum ($\Gamma = 2.8 \pm 0.4$) seen through two distinct layers of absorption of cold gas with column densities of $\sim$7.7 and $\sim$1.5 × 10^{23} cm^{-2}, respectively. However, the spectral parameters of the dual absorber model were largely unconstrained. We then fit the data with the continuum slope fixed to $\Gamma = 1.9$ (as found for the TD model). In this case, the column density of one absorption component was found to be $N_{\rm H} \sim 3.5 \times 10^{23}$ cm^{-2}, while the $N_{\rm H}$ value for the other component was found to be consistent with zero. The ratio of the normalization of two power-law components is $\sim$9.

The hard continuum can also be reproduced with a more complex model where reflection and transmission are both present, which provides a fit with $\chi^2(\nu)$ = 75(72) when both $N_{\rm H}$ and Γ are allowed to vary. The ratio of the normalization of the reflection to that of the transmitted component is $\approx$6, implying that the reflection continuum can easily account for most of the hard X-ray emission in ESO 138−G1. However, we note that the quality of our data, along with the lack of spectral coverage above 10 keV, does not allow to properly constrain the relative contribution of both components. Fixing the value of the column density of the absorber to $N_{\rm H} = 1.6 \times 10^{24}$ cm^{-2} ($=\sigma_t^{-1}$) yields a flattening of the photon index to $\Gamma \sim 1.85$, but does not improve the quality of the fit statistics.

As performed by Guainazzi et al. (2005) and LaMassa et al. (2011) for their samples of heavily obscured Seyfert 2 galaxies, we performed a "local" fit to the spectrum between 5.5 and 7 keV using Cash statistics (Cash 1979), which allows the use of unbinned data without any loss of spectral information, to obtain a more robust determination of the neutral Fe Kα line parameters. The continuum underlying the emission line was modeled with a power law, with the photon index fixed to the best-fit value of $\Gamma = 0.35$. The line energy centroid is at 6.432 ± 0.015 keV, with an upper limit to the line width of $\sigma < 60$ eV. The *EW* measured with respect to the underlying continuum is 790 ± 70 eV (see Table 2), including the contribution from the CS (which originates from Compton backscattering of line photons). By fitting the MOS data, the properties derived for the Fe Kα line are fully consistent with those measured by the PN spectrum.

This value of the *EW* of the 6.4 keV Fe Kα emission line unambiguously rules out the TD scenario (as well as the Compton-thin dual absorber model) because it is too large for a continuum obscured by the Compton-thin column density of a few 10^{23} cm^{-2} derived from the TD fit to the data (e.g., Ghisellini et al. 2004; Guainazzi et al. 2005; Fukazawa et al. 2011). The prominent Fe Kα line observed in ESO 138−G1 lends strong support to the view that the X-ray primary continuum from the AGN is totally depressed in the *EPIC* band, as expected for the presence of a CT absorber, and the 2−10 keV emission is due to the reprocessing of the AGN light by material surrounding the nucleus. Consequently, we adopt hereafter the RD model as the best-fit description of the hard X-ray spectrum of ESO 138−G1.

3.2. Broad-band spectroscopy

As shown in Fig. 1a, the soft X-ray portion of the *XMM-Newton* spectrum of ESO 138−G1 displays several emission features, in addition to a smooth excess below $\sim$3 keV deviating from the flat shape observed for the hard X-ray band. As commonly done for low-resolution spectra of heavily obscured AGNs (e.g., Pounds & Vaughan 2006; Piconcelli et al. 2007), we fitted this "soft excess" with a phenomenological model consisting of the RD model, an unabsorbed power-law component, and a sequence of

Table 2. Best-fit spectral parameters for the emission lines detected in the hard X-ray band.

Line Id. (1)	Energy (2)	*EW* (3)	Intensity (4)
Fe K$\alpha^{\ddagger}$	$6.432^{+0.015}_{-0.015}$	790 ± 70	$2.34 \pm 0.25 \times 10^{-5}$
Fe XXV	$6.63^{\dagger}$	125^{+54}_{-63}	$4.5^{+2.0}_{-2.3} \times 10^{-6}$
Fe Kβ	$7.058^{\dagger}$	80^{+60}_{-70}	$2.3^{+1.7}_{-1.9} \times 10^{-6}$
Ni Kα	$7.54^{\dagger}$	150 ± 90	$2.9 \pm 1.8 \times 10^{-6}$

Notes. See Sect. 3.1 for details. The columns give the following information: (1) line identification; (2) energy (keV); (3) *EW* (eV); and (4) intensity (photons cm^{-2} s^{-1}) of the line. $^{(\ddagger)}$ Properties of the Fe Kα emission line are derived by a "local" fit of the unbinned spectrum in the 5.5−7 keV energy range, using the Cash statistics. The *EW* value includes the contribution of the CS. $^{(\dagger)}$ Fixed value.

narrow Gaussian lines to account for the emission features observed in the ∼0.5−2.5 keV range. The power law was found to be steep ($\Gamma_{\rm soft} = 3.0^{+0.5}_{-0.7}$) and appears to describe a mixture of emissions caused by the electron-scattered fraction of the primary continuum, thermal plasma, and blends of unresolved emission lines and radiative recombination continua, as observed in most X-ray obscured AGNs (Turner et al. 1997; Kinkhabwala et al. 2002). Table 3 lists the best-fit model parameters for the emission lines detected in the soft X-ray band. These emission lines are associated with atomic transitions commonly detected in the soft X-ray spectra of obscured AGNs. However, owing to the limitations imposed by spectral resolution of *EPIC* and potential line blending with adjacent emission lines, both the line identification and parameters should be interpreted with care.

This model provides a good fit to the X-ray spectrum of ESO 138−G1 in the 0.5−10 keV range (Fig. 2), with an associated $\chi^2(\nu) = 156(133)$.

An alternative explanation of the "soft excess" in some obscured AGNs is emission related to star-forming activity. Here we used a combination of two thermal-emission components (`MEKAL` model in XSPEC) to fit the soft X-ray portion of the spectrum of ESO 138−G1. We estimated a metallicity of $Z/Z_{\odot} = 0.3 \pm 0.1$ and a temperature of $kT_1 \approx 0.7$ and $kT_2 < 0.1$ keV, respectively. However, this model yields a poor fit with χ^2_{ν}(d.o.f.) = 1.6(152), leaving significant positive residuals in the 1−2.5 keV region and, thus, disfavoring a scenario wherein the soft excess in ESO 138−G1 originates in thermal emission from a starburst. This is an expected result because a substantial thermal contribution to the soft X-ray emission is typically found only in Seyfert 2/starburst composite galaxies (e.g., Levenson et al. 2001a,b), while the host galaxy of ESO 138−G1 does not exhibit evidence of significant star-forming activity at optical wavelengths (Alloin et al. 1992; Ferruit et al. 2000).

4. Fluxes and luminosities

Once our broad-band best-fit model is assumed, we measure a hard X-ray flux $F_{2-10} = 2.3 \times 10^{-12}$ erg cm^{-2} s^{-1} and a soft X-ray flux $F_{0.5-2} = 3.1 \times 10^{-13}$ erg cm^{-2} s^{-1}. After correction for Galactic absorption, they correspond to an observed luminosity $L_{2-10} = 4.3 \times 10^{41}$ erg s^{-1} and $L_{0.5-2} = 8.8 \times 10^{40}$ erg s^{-1} in the hard and soft band, respectively.

The T ratio of the observed 2−10 keV to the extinction-corrected [OIII] fluxes can be used as a proxy for the amount of obscuration of the X-ray primary continuum, since the [OIII] line is an isotropic indicator of AGN power as it is

Table 3. Best-fit spectral parameters for the emission lines detected in the soft X-ray band.

Energy (1)	Intensity (2)	Identification (3)
0.57 ± 0.02	$5.8^{+2.4}_{-3.0} \times 10^{-5}$	OVII Lyα
0.72 ± 0.01	$3.0 \pm 1.3 \times 10^{-5}$	OVII RRC, Fe XVII 3s-2p
0.84 ± 0.02	$2.5 \pm 0.7 \times 10^{-5}$	Fe XVII-XVIII 3d-2p, OVIII RRC
0.93 ± 0.02	$3.3 \pm 0.9 \times 10^{-5}$	NeIX Heα
$1.02^{\dagger}$	$1.2^{+0.6}_{-0.9} \times 10^{-5}$	NeX Lyα, Fe XXI 3d-2p
1.14 ± 0.03	$9.3 \pm 5.8 \times 10^{-6}$	Fe XXIII-XXIV L
$1.21^{+0.04}_{-0.02}$	$1.1 \pm 0.5 \times 10^{-5}$	NeX Lyβ
1.34 ± 0.02	$1.2^{+0.2}_{-0.3} \times 10^{-5}$	MgXI Heα
1.50 ± 0.02	$6.8^{+1.7}_{-2.0} \times 10^{-6}$	MgXII Lyα
1.82 ± 0.02	$7.6^{+1.4}_{-1.9} \times 10^{-6}$	SXIII Heα
$2.04^{+0.08}_{-0.06}$	$2.0^{+1.3}_{-1.6} \times 10^{-6}$	Si XXIV-XVI Lyα
$2.45^{+0.02}_{-0.03}$	$6.2 \pm 1.8 \times 10^{-6}$	SXV Heα

Notes. See Sect. 3.2 for details. The columns give the following information: (1) energy of the line (keV); (2) intensity of the line (photons cm^{-2} s^{-1}); (3) likely identification (e.g., Brinkman et al. 2002; Guainazzi & Bianchi 2007). $^{(\dagger)}$ indicates that the energy has been fixed to the laboratory energy of NeX Lyα due to the likely superposition of many unresolved Fe lines.

produced in the NLR. In particular, X-ray sources for which $T < 1$ are typically associated with a CT absorber and a 2−10 keV RD spectrum (Bassani et al. 1999; Akylas & Georgantopoulos 2009; Gonzalez-Martin et al. 2009). The extinction-corrected [OIII] flux of ESO 138−G1 is 2.7×10^{-12} erg cm^{-2} s^{-1}, being derived from the observed value of 9.72×10^{-13} erg cm^{-2} s^{-1} reported in Schmitt & Storchi-Bergmann (1995) after the correction (e.g., Lamastra et al. 2009, and references therein) for a Balmer decrement $H_{\alpha}/H_{\beta} = 4.25$ (Alloin et al. 1992). This gives $T = 0.85$, providing further support to the existence of a CT screen that suppresses the observed 2−10 keV flux. Furthermore, in the framework of a TD scenario for the hard X-ray spectrum of ESO 138−G1, we note that the measured value of T is inconsistent with a Compton-thin column density of $\sim 2.5 \times 10^{23}$ cm^{-2}. In this case, the absorption-corrected X-ray flux would be $F_{2-10} = 5.1 \times 10^{-12}$ erg cm^{-2} s^{-1} and, therefore, T is ∼1.9. However, as found by many studies (Maiolino et al. 1998; Panessa et al. 2006; Lamastra et al. 2009), unabsorbed Seyfert 1 and absorption-corrected Compton-thin Seyfert 2 galaxies indeed typically show $T \geq 10$.

5. Discussion

We have presented the analysis of the combined spectroscopic data from two *XMM-Newton* observations of the Seyfert 2 galaxy ESO 138−G1 performed in 2007. The 0.5−10 keV spectrum of this source is typical of a heavily obscured AGN: a very flat hard X-ray continuum with a strong Fe Kα emission line at 6.4 keV and a "soft excess" component characterized by many emission lines from highly ionized metals. In particular, two main pieces of evidence lead us to consider the RD scenario as the most physically plausible description for the *XMM-Newton* data of ESO 138−G1, thus confirm the claim by Collinge & Brandt (2000) based on 1997 *ASCA* data for the existence of a CT absorber covering the primary X-ray continuum in this Seyfert galaxy. The first piece of evidence is the value of *EW* ∼ 800 eV for the Fe Kα line around 6.4 keV. Such a large value cannot be explained if the underlying continuum is transmitted through a Compton-thin absorber

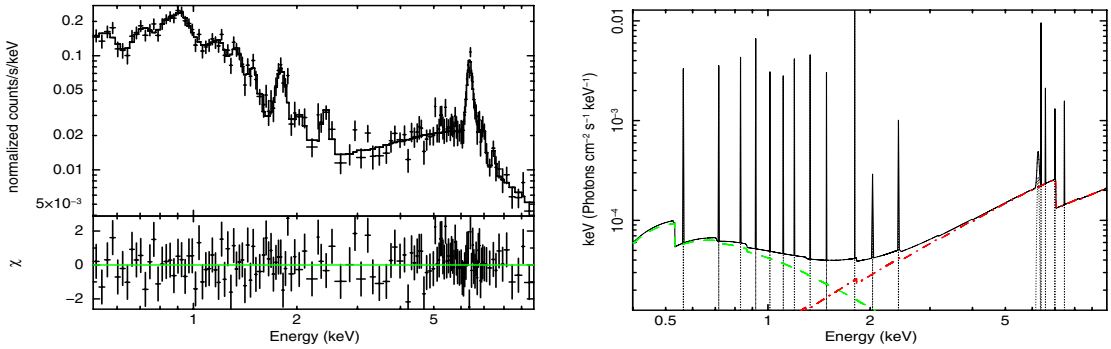

Fig. 2. (a) *Left*: the 0.5−10 keV spectrum of ESO 138−G1 when the best-fit model is applied. The lower panel shows the deviations of the observed data from the model in units of standard deviation. (b) *Right*: best-fit model for the broad band X-ray spectrum. This model (solid line) consists of a pure reflection component (dash-dotted line) plus an additional unobscured power-law component accounting for the soft X-ray scattered/leaked emission (dashed line). It also includes the hard and soft X-ray Gaussian emission lines listed in Tables 2 and 3, respectively.

with $N_{\rm H} \sim 2.5 \times 10^{23}$ cm^{-2}, as inferred by the TD fitting model. A strong Fe Kα emission line with an $EW \gtrsim 0.7-1$ keV is indeed interpreted as the unambiguous signature of a hard X-ray emission produced by reprocessing the intrinsic X-ray continuum and then scattering this radiation along the line of sight (Ghisellini et al. 2004; Guainazzi et al. 2005). In this RD scenario, an obscuring screen with $N_{\rm H} \gtrsim 10^{24}$ cm^{-2} is believed to completely block the X-ray primary source from direct view. It has been generally assumed that the absorber and the reflector consist of the same material, i.e. the *torus*, homogeneously fills a doughnut-shaped region located between the BLR and NLR (Matt et al. 1996; Molendi et al. 2003). However, the discovery of fast transitions from a CT to a Compton-thin spectral state (or vice-versa) have been observed in a handful of Seyfert galaxies (Risaliti et al. 2005; Bianchi et al. 2009) and interpreted in terms of absorbing clouds crossing our line of sight and located very close to the X-ray source (Elitzur 2008). This implies that a line-of-sight clumpy sub-pc-scale absorber exists and, most importantly, the coexistence in the same source of multiple absorbing and/or reflecting components distributed across a range of distances from fractions of pc up to several pc from the SMBH. However, there has so far been no evidence in ESO 138−G1 of large variations in the CT absorber. Future X-ray observations of this source might detect RD to TD spectral state transitions, hence reveal both the presence of an inhomogeneous obscuring gas and the intrinsic luminosity of the X-ray continuum. Finally, the larger EW value of 1.7 ± 0.4 keV for the line at 6.4 keV reported by Collinge & Brandt (2000) can be explained in terms of a blend of the lines associated with Fe Kα emission, caused by the poorer spectral resolution of *ASCA* detector than that provided by the PN camera.

Secondly, the ratio $T = 0.85(1.9)$ of the observed(intrinsic) 2−10 keV flux to the reddening-corrected [OIII] emission line flux is consistent with a RD X-ray spectrum (e.g., Sect. 4), since this value does not agree with those reported for X-ray sources attenuated by a column density $N_{\rm H} < 10^{24}$ cm^{-2} (Maiolino et al. 1988; Bassani et al. 1999; Heckman et al. 2005; De Rosa et al. 2008). Furthermore, the [OIII] luminosity can be used to infer the intrinsic 2−10 keV luminosity of the AGN in ESO 138−G1. Using the Eq. (3) in Lamastra et al. (2009), we derive a $L_{2-10} \approx 6 \times 10^{42}$ erg s^{-1}, i.e. well within the typical Seyfert range (and a factor of six larger than the value inferred by assuming the Compton-thin/TD scenario). The ratio of the value of the intrinsic 2−10 keV luminosity estimated by the [OIII] to the observed value measured from the RD model is ≈14, which is typical of CT AGN (Comastri 2004; Turner et al. 1997). A value of $L_{2-10} \approx 10^{43}$ erg s^{-1} for ESO 138−G1 can also be inferred from its mid-IR luminosity (i.e., $L_{\rm MIR} = 3.46 \times 10^{43}$ erg s^{-1}), as shown by Gandhi et al. (2009). We note that the X-ray luminosity calculated with the TD model, i.e. 9.6×10^{41} erg s^{-1} (see Table 1), is about an order of magnitude lower than this MIR-based estimate.

The estimate of the intrinsic hard X-ray luminosity of ESO 138−G1 allows us to derive some information about the SMBH mass of this object. For a [OIII]-based $L_{2-10} \approx 6 \times 10^{42}$ erg s^{-1}, Vasudevan & Fabian (2007) indicate a bolometric correction of 10. Accordingly, we infer an Eddington luminosity $L_{\rm Edd} = 6 \times 10^{44}$ erg s^{-1} by assuming a ratio $L/L_{\rm Edd} = 0.1$, which is typical of Seyfert galaxies in the local Universe (Woo & Urry 2002). This value of the Eddington luminosity implies a black hole mass of 4.6×10^6 $M_\odot$. It is well-known that near-infrared bulge luminosities and SMBH masses show a tight correlation (e.g., Marconi & Hunt 2003). The K-band magnitude of the bulge of ESO 138−G1 is $K = 10.71$ mag (Peng et al. 2006), which translates into a K-band luminosity of $L_{K,\rm Bulge} = 6.6 \times 10^{10}$ $L_\odot$. Accordingly, we find that ESO 138−G1 does not lie on the $M_{\rm BH} - L_{K,\rm Bulge}$ correlation: the estimated mass of the SMBH is about a factor of ten lower than expected. This implies that ESO 138−G1 is a peculiar early-type galaxy with an undermassive black hole, or an intrinsic X-ray luminosity ten times higher than that estimated based on the [OIII] luminosity, thus providing further support for a CT nature of this AGN.

Finally, useful insights into the nature of the obscuring screen along the line of sight to the nucleus in ESO 138−G1 can also be derived from the 15−150 keV flux level constraint. We note that ESO 138−G1 is indeed included in the catalogs of hard X-ray sources detected by INTEGRAL IBIS (Bird et al. 2010) and Swift BAT (Cusumano et al. 2010) above 15 keV. Specifically, it is associated with the BAT source 2PBC J1651.9−5914, for which $F_{15-150} = 2.3 \pm 0.5 \times 10^{-11}$ erg cm^{-2} s^{-1}, that is centered at a distance of ∼3 arcmin from ESO 138−G1. On the basis of the RD model (i.e. assuming a broad-band, pure reflection spectrum), it is possible to estimate[2] a 15−150 keV flux of $3.1^{+0.1}_{-0.2} \times 10^{-11}$ erg cm^{-2} s^{-1}.

However, since the angular resolution of BAT is ∼20 arcmin *FWHM* and the X-ray loud starburst/Seyfert 2 composite galaxy

[2] We note, however, that any accurate estimate of the reflected emission depends on the geometry of the reflection medium (e.g., Ikeda et al. 2009), which is basically unknown. Meaningful constraints on the geometry of the reprocessor will be possible only using the high signal-to-noise ratio, broad-band spectral data expected from observations performed by *ASTRO-H* and *NuStar* in the near future.

NGC 6221 (e.g., Levenson et al. 2001a) is located at 11 arcmin from our target, the BAT flux can only be used as an upper limit to the X-ray emission from ESO 138−G1 in the 15−150 keV band (La Parola, private communications). The same argument is also valid for the INTEGRAL IBIS flux reported in Bird et al. (2010). We were also able to extract the PN spectrum of NGC 6221, as it falls within the field of view of the detector (although close to the edge) in our observations, to help us determine the possible contribution of this source to the observed BAT flux. The X-ray spectrum of NGC 6221 is well-fitted by a combination of a soft thermal plasma component ($kT \sim 0.6$ keV) and a Compton-thin ($N_{\rm H} \sim 10^{21}$ cm^{-2}) absorbed power law with $\Gamma = 1.6 \pm 0.1$, as found by Levenson et al. (2001a) based on ASCA data[3]. By extrapolating this model to energies >10 keV, we estimate a value of $F_{15-150} = 1.1 \times 10^{-11}$ erg cm^{-2} s^{-1} for the flux in the 15–150 keV band. Therefore, a sizable fraction of the BAT flux ascribed to ESO 138−G1 in the Cusumano et al. catalog might be due to the emission from NGC 6221: in particular, it is likely that the total 15-150 keV flux of $F_{15-150} \approx 2.3 \times 10^{-11}$ erg cm^{-2} s^{-1} seen by BAT and IBIS is produced roughly equally by the two sources. In turn, this may indicate that the column density of the nuclear absorber in ESO 138−G1 should be $N_{\rm H} \gtrsim 10^{25}$ cm^{-2}, otherwise any additional emission component in the 15−150 keV band caused by the X-ray primary continuum transmitted through an absorber with $N_{\rm H} \sim$ a few 10^{24} cm^{-2}, would produce a further increase in the final flux, significantly exceeding the IBIS/BAT flux values.

In this respect, future observations of ESO 138−G1 above 10 keV will be crucial to shed light on the properties of the X-ray continuum emission and the obscuring gas in the nuclear environment of this Seyfert 2 galaxy. We note, however, that given the proximity of NGC 6221, low-resolution (i.e. with $FWHM \gg 10$ arcmin) observations carried out with current X-ray observatories such as Swift BAT, INTEGRAL IBIS and *Suzaku* PIN cannot provide an unambiguous and definitive test of whether ESO 138−G1 contains a heavily CT (i.e. $N_{\rm H} \gg 10^{24}$ cm^{-2}) absorber. This will be achieved by next generation X-ray missions such as NuSTAR (Harrison et al. 2010) and ASTRO-H (Takahashi et al. 2010), which should to fly in 2012 and 2014, respectively, as they combine ∼50−90 arcsec imaging with high spectral resolution in the ∼10−60 keV energy range.

The soft portion of the X-ray spectrum of ESO 138−G1 shows the typical properties of other obscured AGNs, with the presence of a highly structured "soft excess". High-resolution imaging and spectroscopy of Seyfert 2 galaxies performed with *XMM-Newton* and *Chandra* have allowed us to reveal that the soft X-ray spectrum originates from extended emission photoionized by the AGN (Kinkhabwala et al. 2002; Bianchi et al. 2006; Guainazzi & Bianchi 2007). The contribution of collisionally ionized plasma associated with starburst regions does not appear to be significant, except in objects known to host intense star-formation activity, such as highly disturbed systems and very luminous IR galaxies (Netzer et al. 2005; Guainazzi et al. 2009; Piconcelli et al. 2010). Narrow-band [OIII] images of ESO 138−G1 show a jet-like feature extending up to ≈2 kpc westwards from the center, produced by the ionizing nuclear radiation (Schmitt & Storchi-Bergmann 1995). Furthermore, high-resolution near-UV and [OIII] images of ESO 138−G1 taken with the ACS and WFPC2 detectors onboard HST (Munoz-Marin et al. 2007; Ferruit et al. 2000) have revealed a bright, ionization cone-shaped circumnuclear zone (∼200 pc) of diffuse light. Close morphological correspondences between the soft X-ray and the [OIII] emission on a kpc scale are frequently observed in heavily obscured Seyfert 2 galaxy and clearly indicate a common physical origin (i.e. photoionization) for the two emissions (Brinkman et al. 2002; Bianchi et al. 2006, and references therein). Accordingly, we suggest that this may turn out to also be the case for the origin of the line-rich "soft excess" observed in the *XMM-Newton* spectrum of ESO 138−G1. However, high-resolution X-ray spectroscopy and imaging with deep exposures of ESO 138−G1 are needed to unambiguously confirm the presence of photoionized gas in this Seyfert 2 galaxy and resolve its morphological details.

[3] The 2−10 keV flux of NGC 6221 measured by the *XMM-Newton* observation is $F_{2-10} \sim 3 \times 10^{-12}$ erg cm^{-2} s^{-1}, i.e. a factor of 4.5 lower than the value derived by previous *ASCA* data, thus confirming the presence of large flux variability in this source as reported in Levenson et al. (2001b).

Acknowledgements. We thank the referee for comments that helped to improve the clarity of this manuscript. We would like to thank the staff of the *XMM-Newton* Science Operations Center for their support. We thank Valentina La Parola for her help in the discussion about Swift BAT observations. E.P., S.B., and C.V. acknowledge support under ASI/INAF contracts I/088/06/0 and I/009/10/0. Based on observations obtained with *XMM-Newton*, an ESA science mission with instruments and contributions directly funded by ESA Member States and NASA. This research has made use of the NASA/IPAC Extragalactic Database (NED) which is operated by the Jet Propulsion Laboratory, California Institute of Technology, under contract with the National Aeronautics and Space Administration.

References

Akylas, A., & Georgantopoulos, I. 2009, A&A, 500, 999
Alloin, D., Bica, E., Bonatto, C., & Prugniel, P. 1992, A&A, 266, 117
Arnaud, K. A. 1996, ASPC, 101, 17
Avni, Y. 1976, ApJ, 210, 642
Bassani, L., Dadina, M., Maiolino, R., et al. 1999, ApJS, 121, 473
Bianchi, S., Guainazzi, M., & Chiaberge, M. 2006, A&A, 448, 499
Bianchi, S., Chiaberge, M., Piconcelli, E., & Guainazzi, M. 2007, MNRAS, 374, 697
Bianchi, S., Piconcelli, E., Chiaberge, M., et al. 2009, ApJ, 695, 781
Bird, A. J., Bazzano, A., Bassani, L., et al. 2010, ApJS, 186, 1
Brandt, W. N., & Alexander, D. M. 2010, PNAS, 107, 7184
Brinkman, A. C., Kaastra, J. S., van der Meer, R. L. J., et al. 2002, A&A, 396, 761 0
Burlon, D., Ajello, M., Greiner, J., et al. 2011, ApJ, 728, 58
Cappi, M., Panessa, F., Bassani, L., et al. 2006, A&A, 446, 459
Cash, W. 1979, ApJ, 228, 939
Collinge, M. J., & Brandt, W. N. 2000, MNRAS, 317, L35
Comastri, A. 2004, ASSL, 308, 245
Cusumano, G., La Parola, V., Segreto, A., et al. 2010, A&A, 524, A64
Comastri, A., Ranalli, P., Iwasawa, K., et al. 2011, A&A, 526, L9
de Rosa, A., Bassani, L., Ubertini, P., et al. 2008, A&A, 483, 749
den Herder, J. W., Brinkman, A. C., Kahn, S. M., et al. 2001, A&A, 365, L7
Elitzur, M. 2008, New Astron. Rev., 52, 274
Ferruit, P., Wilson, A. S., & Mulchaey, J. 2000, ApJS, 128, 139
Feruglio, C., Daddi, E., Fiore, F., et al. 2011, ApJ, 729, L4
Fiore, F., Puccetti, S., Grazian, A., et al. 2011, A&A, in press [arXiv:1109.2888]
Fukazawa, Y., Hiragi, K., Mizuno, M., et al. 2011, ApJ, 727, 19
Gabriel, C., Denby, M., Fyfe, D. J., Hoar, J., & Ibarra, A. 2004, in Astronomical Data Analysis Software and Systems XIII, ed. F. Ochsenbein, M. Allen, & D. Egret (San Francisco: ASP), ASP Conf. Ser., 314, 759
Gandhi, P., Horst, H., Smette, A., et al. 2009, A&A, 502, 457
Ghisellini, G., Haardt, F., & Matt G. 1994, MNRAS, 267, 743
Gilli, R., Comastri, A., & Hasinger G. 2007, A&A, 463, 79
Gilli, R., Su, J., Norman, C., et al. 2011, ApJ, 730, L28
González-Martín, O., Masegosa, J., Márquez, I., & Guainazzi, M. 2009, ApJ, 704, 1570
Guainazzi, M., Matt, G., & Perola G. C. 2005, A&A, 444, 119
Guainazzi, M., & Bianchi, S. 2007, MNRAS, 374, 1290
Guainazzi, M., Risaliti, G., Nucita, A., et al. 2009, A&A, 505, 589
Halpern, J. P., Turner, T. J., & George I. M. 1999, MNRAS, 307, L47
Harrison, F. A., Boggs, S., Christensen, F., et al. 2010, SPIE, 7732, 77320S
Heckman, T. M., Ptak, A., Hornschemeier, A., & Kauffmann G. 2005, ApJ, 634, 161

Ikeda, S., Awaki, H., & Terashima, Y. 2009, ApJ, 692, 608
Jansen, F., Lumb, D., Altieri, B., et al. 2001, A&A, 365, L1
Kalberla, P. M. W., Burton, W. B., Hartmann, D., et al. 2005, A&A, 440, 775
Kinkhabwala, A., Sako, M., Behar, E., et al. 2002, ApJ, 575, 732
LaMassa, S. M., Heckman, T. M., Ptak, A., et al. 2011, ApJ, 729, 52
Lamastra, A., Bianchi, S., Matt, G., et al. 2009, A&A, 504, 73
Larson, D., Dunkley, J., Hinshaw, G., et al. 2011, ApJS, 192, 16
Levenson, N. A., Cid Fernandes, R. Jr., Weaver, K. A., Heckman, T. M., & Storchi-Bergmann, T. 2001a, ApJ, 557, 54
Levenson, N. A., Weaver, K. A., & Heckman, T. M. 2001b, ApJS, 133, 269
Magdziarz, P., & Zdziarski, A. A. 1995, MNRAS, 273, 837
Maiolino, R., Salvati, M., Bassani, L., et al. 1998, A&A, 338, 781
Malizia, A., Stephen, J. B., Bassani, L., et al. 2009, MNRAS, 399, 944
Marconi, A., & Hunt, L. K. 2003, ApJ, 589, L21
Marconi, A., Risaliti, G., Gilli, R., et al. 2004, MNRAS, 351, 169
Matt, G. 1997, MmSAI, 68, 127
Matt, G. 2002, MNRAS, 337, 147
Muñoz Marín, V. M., González Delgado R. M., Schmitt H. R., et al. 2007, AJ, 134, 648
Netzer, H., Lemze, D., Kaspi, S., et al. 2005, ApJ, 629, 739
Panessa, F., Bassani, L., Cappi, M., et al. 2006, A&A, 455, 173
Peng, Z., Gu, Q., Melnick, J., & Zhao, Y. 2006, A&A, 453, 863
Piconcelli, E., Jimenez-Bailón, E., Guainazzi, M., et al. 2004, MNRAS, 351, 161
Piconcelli, E., Bianchi, S., Guainazzi, M., Fiore, F., & Chiaberge M. 2007, A&A, 466, 855
Piconcelli, E., Vignali, C., Bianchi, S., et al. 2010, ApJ, 722, L147
Pounds, K., & Vaughan, S. 2006, MNRAS, 368, 707
Ramos-Almeida, C., Levenson, N. A., Rodriguez Espinosa, J. M., et al. 2009, ApJ, 702, 1127
Risaliti, G., Maiolino, R., & Salvati, M. 1999, ApJ, 522, 157
Risaliti, G., Elvis, M., Fabbiano, G., Baldi, A., & Zezas, A. 2005, ApJ, 623, L93
Sambruna, R. M., Brandt, W. N., Chartas, G., et al. 2001, ApJ, 546, L9
Schmitt, H. R., & Storchi-Bergmann, T. 1995, MNRAS, 276, 592
Takahashi, T., Mitsuda, K., Kelley, R., et al. 2010, SPIE, 7732, 77320Z
Turner, T. J., George, I. M., Nandra, K., & Mushotzky, R. F. 1997, ApJS, 113, 23
Vasudevan, R. V., & Fabian, A. C. 2007, MNRAS, 381, 1235
Woo, J.-H., & Urry, C. M. 2002, ApJ, 579, 530
Worsley, M. A., Fabian, A. C., Bauer, F. E., et al. 2005, MNRAS, 357, 1281
Yaqoob, T., & Murphy, K. D. 2011, MNRAS, 412, 277